WILEY-VCH

DOI: 10.1002/ ((please add manuscript number))
Article type: Communication

Title: Mixed-mode electro-optical operation of $Ge_2Sb_2Te_5$ nanoscale crossbar devices.

*Gerardo Rodriguez-Hernandez, Peiman Hosseini, Carlos Ríos, C. David Wright and Harish Bhaskaran**

G. Rodriguez-Hernandez, Dr P. Hosseini, C. Ríos, Prof. H. Bhaskaran
Advanced Nanoscale Engineering Group, Department of Materials, University of Oxford, Parks Road, OX1 3PH, Oxford, UK
E-mail: harish.bhaskaran@materials.ox.ac.uk
Prof. C.D. Wright
Department of Engineering, University of Exeter, Streatham Campus, Harrison Building, North Park Road, EX4 4QF, Exeter, UK

Keywords: phase-change photonics, optoelectronics, nano-devices, phase-change materials

The use of phase-change materials for a range of exciting new optoelectronic applications from artificial retinas to ultra-high resolution displays require a thorough understanding of how these materials perform under a combination of optical and electrical stimuli. Herein we report for the very first time the complex link between the electronic and optical properties in real-world crossbar nanoscale devices constructed by confining a thin layer of $Ge_2Sb_2Te_5$ between transparent ITO electrodes, forming an optical nano-cavity. We present a novel proof-of-concept device that can be operated by a combination of optical and electrical stimuli, leading the way for the development of further applications based on mixed-mode electro-optical operation.

1. Introduction

Chalcogenide-based phase-change materials have been the subject of much scientific interest because of their ability to reversibly switch between two solid states, amorphous and crystalline, at high speed[1] and with relatively low power consumption[2]. Transitions between states are achieved via localized heating with energy applied either optically or as an electrically [3]. One of the most common phase-change materials is $Ge_2Sb_2Te_5$ (GST). Each of the atomic configurations of GST have different physical (optical, electrical and mechanical) properties[4]. The crystalline phase is more reflective and up to three orders of magnitude more electrically conductive than the amorphous phase [1]. These differences in the physical properties between phases, in addition to the ability to retain either phase state for a long time at ambient temperatures[5], have been utilized in technologies such as rewritable optical data storage (DVD-RW, Blu-ray RW)) and nonvolatile electronic phase-change memories (PCMs)[6]. Exploiting both optical and electrical properties of phase-change materials simultaneously, and the possibility of modulating optical effects using electrical excitations, has only very recently opened up new application fields, such as low-power, non-volatile, phase-change nano-displays[7][8][9]. A deeper understanding of the relationship between the optical and electrical properties of phase-change materials, such as GST, is now urgently required to spur the development of new optoelectronic applications.

Some previous studies have examined the basic relationship between reflectance and electrical resistance of phase-change materials. For instance, by comparing the crystallization times of $Ge_{15}Sb_{85}$ in planar films excited optically and in bridge nanodevices excited electrically, it was shown that optical and electrical properties are interrelated[10]. Furthermore, simultaneous measurements of reflectivity and electrical resistivity of GST thin films during isothermal crystallization showed a decrease in resistivity preceding an increase in reflectivity,

explained by the appearance of small crystalline nuclei that enable electrical conduction by percolation prior to the formation of a crystalline region large enough to be optically detectable[11]. Similar observations have been reported by measuring the transient crystallization response of as-deposited-amorphous GST exposed to single-nanosecond laser pulsed excitations [12].

In the above mentioned works, films were driven from fully amorphous to fully crystalline by applying either a continuous heat source or laser pulse. However, intermediate partially crystalline states can of course also exist. In particular, GST allows for the existence of nanometer-sized crystalline nuclei in the amorphous phase by having a nucleation dominated crystallization mechanism[13]. The eventual increase in the size and number of crystalline nuclei usually accounts for the transition to the fully crystalline state. Therefore, by applying a series of pulses with a controlled amount of energy, it is possible to transition between fully amorphous and fully crystalline states in discrete incremental steps. This property has been referred to as *accumulation*, and occurs by means of optical as well as electrical pulses[14][15][16]. In this work therefore we investigate the phase transition of GST by simultaneously examining the optical and electrical responses of crossbar-type nanoscale devices exposed to cumulative optical and electrical excitations.

2. Methodology

In order to apply laser pulses and measure the reflectance of the samples, we used a custom-built reflective laser scanning microscope (**Figure 1**a). A 658nm (red) laser diode (ROHM RLD65PZB5) is coupled to a single mode optical fibre using an aspheric lens coupler/collimator (Thorlabs F280APC-B). Once coupled, the beam passes through a 90:10 fibre beam splitter (Thorlabs FC632-90B-APC) that allows the reflected signal to be sensed by a photo detector (New Focus 2001). The scanning objective was built in a confocal configuration by assembling a ferrule terminated single mode optical fibre (Thorlabs

SMPF0206-APC) to a 0.29 pitch grin lens (Thorlabs GRIN2906). This configuration allows the fibre to be used as a pinhole[17] in the path of the reflected light. The optimum values for the trade-off between working distance and spot size were calculated following a transfer matrix model[18] and set to 328 μm and 2.24 μm respectively. The scanning objective was mounted on top of the precision XY piezo stage of an Asylum MFP-3D Atomic Force Microscope using a custom-built base in contact to the XY piezo by a three groove kinematic clamp. By using the MFP-3D AFM it is possible to perform the XY movements to construct the image, as well as to use one of the integrated AFM Analog/Digital converters to acquire the photo detector signal simultaneously with the raster scan. Such synchronization allows for precise positioning of the laser beam subsequently to the scan. The focus of the laser spot on the sample (Z axis) was controlled by a combination of a manual linear stage (Thorlabs DT12/M) for coarse adjustment and a custom-built multi-element piezo linear actuator[19] for fine adjustment. Essentially, we adapted the extremely fine linear (x-y) piezo of our Asylum AFM to our home-built optical probe, in order to optically test our devices. Similar laser probing configurations have been reported previously in the literature[20]. In this case however, we used fibre coupled optical components in order to reduce the footprint of the custom made laser accessory so it could be accommodated in the existing MPF-3D AFM system.

For our experiments we fabricated crossbar nanoscale devices following the process shown in Fig. 1b-j, with ITO transparent electrodes which confine a small GST area forming an optical nano cavity that is accessible optically and electrically. Starting with a thermally oxidized Si wafer (320nm SiO_2) (Fig. 1b) and by employing a bi-layer positive resist (PMMA 495 + PMMA950) (Fig. 1c), the bottom electrode design was patterned by e-beam lithography (Fig. 1d). After development, reactive ion etching (RIE) was used to produce 20 nm deep trenches in the SiO_2. The trenches were then filled with 20 nm Indium Tin Oxide (ITO) deposited by RF plasma sputtering (Fig. 1e). After lift-off, the sample was annealed at 300°C for 30 minutes in air, to improve the conductivity of the ITO bottom electrode. The trenches in

the SiO_2 substrate serve as a simple planarization mechanism, which is used to increase the yield of the devices by avoiding short-circuit between the top and bottom electrodes in the cross bar structure, in addition to improving thermal properties of the device. A second e-beam lithography process was used to pattern the top part of the cross bar device (Fig. 1f-g). In this case a 15 nm thin-film of GST was deposited by RF sputtering, followed by 20 nm of ITO that serves as the transparent top electrode. Both materials were deposited within the same deposition run, avoiding the GST being exposed to oxygen from air (Fig. 1h). Then, a set of larger electrodes were added to access the device electrically. These electrodes were created by a third e-beam lithography process followed by thermal evaporation of 30 nm Cr as an adhesive layer followed by 60 nm Au. The considerable thickness of the Cr adhesive layer (30nm) was used to improve the electrical contact between the ITO and the Au electrodes[21]. A batch of 48 devices of each size 100nm, 200nm, 300nm, 500nm and 1µm were fabricated simultaneously during the fabrication process, it was found during characterization that 500nm and 1µm gave the better response in terms of reliability and optical response and were therefore used for our experiments. Finally, electrical access to the devices was achieved by wire bonding each device to a chip carrier. The chip carrier was mounted on a custom-made magnetic holder designed to firmly fix the device in place during the raster scan of the laser microscope. Electrical measurements were performed with a source meter (Keithley 2614B).

It is known that thermal characteristics play an important role in the operation of phase-change memories[22]. Good heat containment accounts for more efficient devices, by reducing thermal losses. The use of ITO electrodes in the present design serves two purposes: it enhances thermal isolation because of its low thermal conductivity, ~11 W/mK, compared to metallic electrodes while simultaneously allowing optical access to measure the changes in reflectance induced by the change of phase of the GST layer.

3. Results and Discussion

Three combined mixed-mode experiments were carried out to explore the simultaneous electrical and optical behavior of phase-change materials (in this case GST) in a nanoscale device context. The first experiment was to ascertain how optical pulses would modulate the resistance of the devices. We subjected our devices to a series of optical pulses to induce crystallization; the resistance of the device was then measured after each optical pulse. The optical pulses were 50 ns in duration and 13 mW in power (output power radiated from the grin lens), a combination that allows for a steady progression from the initial as-deposited amorphous state to the crystalline phase. **Figure 2a** shows the evolution of the resistance for two devices of dimensions 500 nm x 500 nm and 1 µm x1 µm. As it can be seen, the resistance value in both devices gradually drops, by approximately three orders of magnitude in this case, as the cumulative effects of the optical pulses lead to crystallization. It is important to notice that despite the large change, the device is highly resistive at all times (approximately 1MΩ in the low value) this is caused by the parasitic resistance of the ITO electrodes. As the GST becomes more crystalline, the electrical resistance decreases in both devices of different sizes. The difference in the accumulative response of both devices is due to an increase of the thermal losses associated with wider electrodes. Therefore the optical pulses applied to the larger device were less effective in inducing crystallization, and more were required to reach the lowest resistive level.

In the second experiment we examine how electrical excitation pulses affect the optical properties, specifically the reflectance, of a device. We thus applied a series of electrical pulses to a 500 nm x500 nm crossbar cell, measuring its resistance and reflectance after each pulse. The applied voltage pulses were of 2.5 V and 100 ns duration, which again allows for a steady accumulative phase transition. Our optical measurements were performed by acquiring sequential images with our laser scanning microscope using a low intensity laser beam of 1 mW. The images were then post-processed following the methodology described in section 1

of the supplementary information (using such a methodology serves two purposes: first, after every scan it is possible to re-position the laser before applying the next pulse in case of unexpected stage drift; second, we can use the imaged substrate reflectance as a reference to compensate for laser intensity variations).

Figure 2b shows the evolution of the reflectance and resistance of the crossbar device as a function of the number of electrical pulses applied. The electrical resistance drops as the number of pulses increases, as would be expected for a device undergoing crystallization via an accumulation process. Surprisingly however, the reflectance of the devices decreases with increasing number of applied pulses. This behavior is counter-intuitive, given that it is known that the reflectance of blanket GST films increases upon crystallization for wavelengths in the visible spectrum[23]. In this case however, such response is a consequence of a shift, upon partial crystallization, in the resonance of the optical cavity formed by stacking the different layers (ITO/GST/ITO) that form the cell. This shift is produced by the change of the refractive index of the GST upon partial crystallization[7] (for more information see section 2 of the supplementary).

It can also be seen in Fig. 2b that the evolution of the reflectance occurs before the final resistance drop. The fact that both measurements evolve differently suggests that the crystallization of the GST within the device may not be occurring homogeneously. These findings are similar to the previously observed by Liang et. al.[12], who explained a delay in the evolution of the reflectance respect to the resistance by a two-dimensional percolation model.

Thus far, we have shown that subjecting the GST crossbar cell to optical pulses produces an observable change in resistance and that electrical pulses produce and observable change in reflectance. However, in order to further understand the relationship between the changes of these two physical properties we performed an additional experiment applying a series of 50 ns, 13 mW optical pulses to a 500 nm x 500 nm device and measured both the resistance and the reflectance after each pulse. These results are shown in **Figure 3a.** The graph has been divided

into sections, and each section has been selected to highlight how the trends of the reflectance and resistance changes are either opposite or in tandem to each other as the GST freely changes phase.

In these results, the change in reflectance follows a similar behavior to the one observed in the previous experiment (Figure 2b). As explained before, the reflectance initially decreases upon partial crystallization due to the resonance change of the optical nano-cavity caused by the change of the refractive index of GST. Figure 3b shows the simulated non-monotonic optical response at 658nm of the optical nano-cavity as a function of the crystalline fraction.

This curve is divided into two regions: in region (I) the reflectance decreases as the GST partially crystallizes, in region (II) a further increase of crystallization induces an increase in reflectance, reaching the peak value when the GST becomes fully crystalline. Given that an increasing crystallization fraction will produce a monotonic decrease of resistance, as was shown previously in Figure 2a, within region (I) the trends in the change of resistance and reflectance will be opposite to each other, whereas in region (II) they will be the same. Thus, different degrees of crystallization are responsible for the changes shown in the various regions (A-K) of Figure 3a, as the GST in the device traverses between regions (I) and (II) of the optical response shown in Figure 3b. This remarkable optoelectronic response is a consequence of the optical resonance characteristics of the optical nano-cavity formed by the crossbar cell, along with the fact that, for the particular optical excitation pulses used here, the cell 'oscillates' between regions (I) and (II) due to a process of partial crystallization and partial re-amorphization induced by successive excitations in tandem with the change in absorbance of GST between amorphous and crystalline states[24] (this can be inferred from the observation that the partial reamorphization takes place only after sufficient crystallization has occurred - see Figure 3a, region A).

Up to this point, we have shown that a correspondence exists between resistance and reflectance when either optical or electrical excitation pulses are applied, and that such

correspondence depends on the degree of partial crystallization. In our third experiment we demonstrate true combined electro-optical operation of our devices (mixed-mode) at the nanoscale. A 500 nm x 500 nm device was conditioned optically until it reached the lowest resistance state. We then iteratively applied a series of 50 optical pulses of 80 ns at 65 mW of optical power (measured at the GRIN lens output) to re-amorphize the GST, followed by an incremental staircase voltage signal (Figure S4 of the supplementary information) from 0 to 4 V to electrically crystallize the material again.

Figure 4 shows the result of 10 iterations of our mixed-mode experiment. It is seen that after the application of a series of optical pulses, an increment in the resistance is observed. Similarly, after an electrical triangular staircase signal is applied, the resistance decreases again as the GST re-crystallizes. The change of the resistance is approximately one order of magnitude, which is significantly less than the change observed in the first transition from as-deposited amorphous state reported previously in Figures 1 and 2. Also the operation occurs in the lower range of the resistance, near the fully crystalline region. Both of these indicate that the optical pulses do not fully re-amorphize the material (See Section 4 of the supplementary information). However, partial re-amorphization does occur and modulates the resistance, demonstrating mixed-mode operation for the very first time in nanoscale devices. We repeated the behavior seen in Figure 4 for over 100 iterations.

4. Conclusion

In conclusion, we have experimentally shown for the very first time in nanoscale GST phase-change devices that there exists a complex relationship between the resistance, reflectance and crystallinity of the GST. Such a relationship exists irrespective of the means used to induce the crystallization (i.e. electrical or optical pulses). An optically induced phase-change can readily produce a change in device resistance while at the same time an electrically induced phase-change can be observed as a change in reflectance. We have also shown that partial crystallization due to accumulation of pulses occurs, and we suggest that partial

crystallization of the GST within our mixed-mode device is not homogeneous. Further investigation is required to understand whether crystalline and amorphous phase segregation occur within the device, in order to optimize the optical contrast and energy required for the operation. Moreover, we have provided a proof-of-concept GST nanodevice in mixed-mode electro-optical operation by crystallizing it electrically and re-amorphizing it optically while the resistance values show two different repeatable states. Our results are a first step towards the realization of a memflector[25] (the optoelectronic analogue of the memristor), as well as other optoelectronic devices for future applications that require a memory element capable of operating electrically and optically. Such applications include optoelectronic interfaces for integrated photonic circuits[26][27], in addition to potential new technologies like accumulative optical pulse detectors or synthetic retinas.

5. Experimental Section

E-beam lithography: We used a Jeol-5500 Series E-beam lithography tool and a PMMA bilayer resist (PMMA495 + PMMA950). The final lithographic step to create access electrodes used a single PMMA495 resist layer.

RIE etching: At a base pressure of $5x10^{-6}$ mTor, we etched 20 nm of $Si0_2$ using 25sccm CHF_3 + 25sccm Ar, and an operating pressure of 30 mTor for 1 min @ 200W.

Bottom electrode Deposition: This was carried out in a Nordiko system; ITO was sputtered from a 2 inch target (Testbourne, UK) with a base pressure of $1x10^{-7}$mbar, operating pressure of $7x10^{-3}$ mbar, 100 sccm Ar @ 30 W for 9 min 30 s.

RF sputtering GST/ ITO top electrode: $Ge_2Sb_2Te_5$ was sputtered from a 2 in target (Super Conductor Materials, USA) with a base pressure of $1x10^{-7}$ mbar, a chamber pressure of $7x10^{-3}$ mbar, flow of 100 sccm Ar, at a power of 30W for 4 min 10 secs. The ITO top electrode was then sputtered in-situ, with the same parameters as bottom ITO electrode.

Thermal evaporation: 30nm of Cr + 60nm Au was evaporated from a Cr rod and Au wire on W crucible, respectively, at rate of 0.1nm/sec monitored by a crystal deposition monitor. Chamber base pressure was $2x10^{-6}$ mbar.

Supporting Information
Supporting Information is available from the Wiley Online Library or from the author.

Acknowledgements

G.R.H. Thanks the support of CONACYT, Mexican Government for the Student Grant 215365. All authors acknowledge support from EPSRC via grants EP/J018783/1, EP/M015173/1 and EP/M015130/1. HB acknowledges support from an EPSRC Manufacturing Fellowship EP/J018694/1.

Received: ((will be filled in by the editorial staff))
Revised: ((will be filled in by the editorial staff))
Published online: ((will be filled in by the editorial staff))

[1] J. Siegel, A. Schropp, J. Solis, C. N. Afonso, M. Wuttig, *Appl. Phys. Lett.* **2004**, *84*, 2250.

[2] F. Xiong, A. D. Liao, D. Estrada, E. Pop, *Science* **2011**, *332*, 568.

[3] M. Wuttig, N. Yamada, *Nat. Mater.* **2007**, *6*, 824.

[4] A. Chabli, C. Vergnaud, F. Bertin, V. Gehanno, B. Valon, B. Hyot, B. Bechevet, M. Burdin, D. Muyard, *J. Magn. Magn. Mater.* **2002**, *249*, 509.

[5] A. Pirovano, A. L. Lacaita, A. Benvenuti, F. Pellizzer, S. Hudgens, R. Bez, In *IEEE International Electron Devices Meeting*; IEEE, 2003; pp. 29.6.1–29.6.4.

[6] N. Yamada, *Phys. Status Solidi* **2012**, *249*, 1837.

[7] P. Hosseini, C. D. Wright, H. Bhaskaran, *Nature* **2014**, *511*, 206.

[8] C. Ríos, P. Hosseini, R. A. Taylor, H. Bhaskaran, *Adv. Mater.* **2016**, *28*, 4720.

[9] P. Hosseini, H. Bhaskaran, In *SPIE 9520, Integrated Photonics: Materials, Devices, and Applications III*; Fédéli, J.-M., Ed.; Barcelona, Spain, 2015; Vol. 9520, p. 95200M.

[10] D. Krebs, S. Raoux, C. T. Rettner, G. W. Burr, R. M. Shelby, M. Salinga, C. M. Jefferson, M. Wuttig, IBM/Macronix PCRAM Joint Project, *J. Appl. Phys.* **2009**, *106*, 054308.

[11] D.-H. Kim, F. Merget, M. Laurenzis, P. H. Bolivar, H. Kurz, *J. Appl. Phys.* **2005**, *97*, 083538.

[12] G. Liang, K. Zhang, F. Zhai, H. Huang, Y. Wang, Y. Wu, *Chem. Phys. Lett.* **2011**, *507*, 203.

[13] D. Lencer, M. Salinga, M. Wuttig, *Adv. Mater.* **2011**, *23*, 2030.

[14] C. D. Wright, P. Hosseini, J. A. Vazquez Diosdado, *Adv. Funct. Mater.* **2013**, *23*, 2248.

[15] C. D. Wright, Y. Liu, K. I. Kohary, M. M. Aziz, R. J. Hicken, *Adv. Mater.* **2011**, *23*,

3408.

[16] P. Hosseini, A. Sebastian, N. Papandreou, C. D. Wright, H. Bhaskaran, *IEEE Electron Device Lett.* **2015**, *36*, 975.

[17] P. M. Delaney, M. R. Harris, R. G. King, *Appl. Opt.* **1994**, *33*, 573.

[18] W. Jung, W. Benalcazar, A. Ahmad, U. Sharma, H. Tu, S. A. Boppart, *J. Biomed. Opt.* **2010**, *15*, 066027.

[19] W.-M. Wang, K.-Y. Huang, H.-F. Huang, I.-S. Hwang, E.-T. Hwu, *Nanotechnology* **2013**, *24*, 455503.

[20] H.-K. Ji, H. Tong, H. Qian, Y.-J. Hui, N. Liu, P. Yan, X.-S. Miao, *Sci. Rep.* **2016**, *6*, 39206.

[21] B. Moazzez, S. M. O'Brien, E. F. S. Merschrod, *Sensors (Switzerland)* **2013**, *13*, 7021.

[22] S. Raoux, F. Xiong, M. Wuttig, E. Pop, *MRS Bull.* **2014**, *39*, 703.

[23] S.-Y. Kim, S. J. Kim, H. Seo, M. R. Kim, In *Proc. SPIE 3401,Optical Data Storage*; Kubota, S. R.; Milster, T. D.; Wehrenberg, P. J., Eds.; SPIE Press: Aspen, 1998; pp. 112–115.

[24] H. Huang, F. Zuo, F. Zhai, Y. Wang, T. Lai, Y. Wu, F. Gan, *J. Appl. Phys.* **2009**, *106*, 063501.

[25] C. D. Wright, L. Wang, M. M. Aziz, J. a. V. Diosdado, P. Ashwin, *Phys. Status Solidi* **2012**, *249*, 1978.

[26] C. Rios, P. Hosseini, C. D. Wright, H. Bhaskaran, W. H. P. Pernice, *Adv. Mater.* **2013**.

[27] C. Ríos, M. Stegmaier, P. Hosseini, D. Wang, T. Scherer, C. D. Wright, H. Bhaskaran, W. H. P. Pernice, *Nat. Photonics* **2015**, *9*, 725.

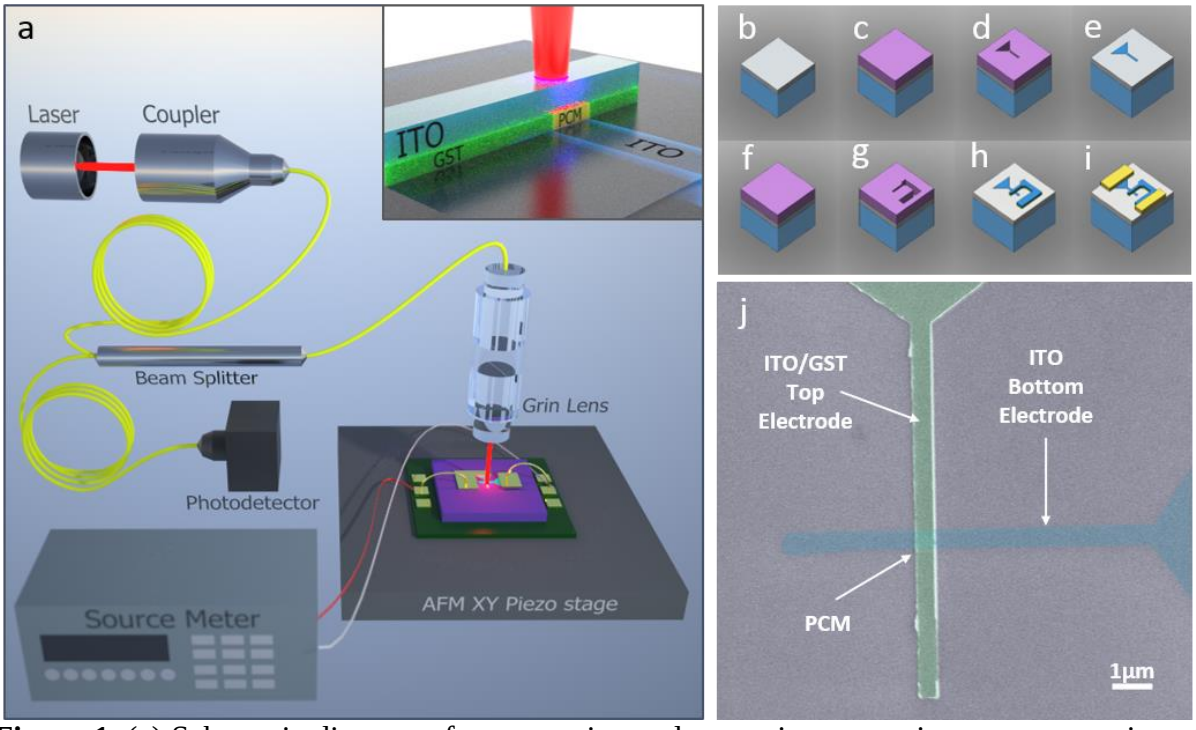

Figure 1. (a) Schematic diagram of our experimental setup, inset contains a representation of the optical nano-cavity formed by the different layers of the crossbar device (not to scale). (b-

i) Fabrication steps of crossbar nano-devices; (b)Initial Si/SiO2 wafer, (c) bi-layer PMMA resist (495+950), (d) e-beam patterning and development of bottom electrode design, this mask is used for Reactive Ion Etching (RIE) of trenches, later the trenches are filled with ITO deposited by RF sputtering, (e)completed bottom electrode after lift-off, (f)second bi-layer PMMA resist(495+950), (g)e-beam patterning and sputtering of GS/ITO layers to form the top electrode, (h) top and bottom electrodes completed after lift-off of the top electrode mask, (i) Cr/Au access electrodes are added to complete the device. (j) Digitally colored SEM picture of a completed 500x500 nm^2 crossbar nano-device, inset describes the optical stack formed by the crossbar area.

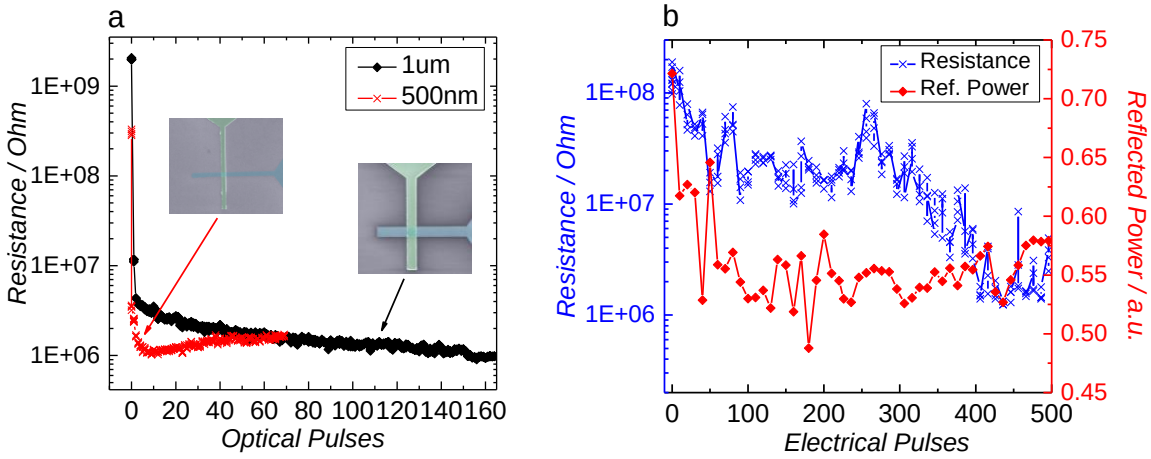

Figure 2. a) Evolution of electrical resistance in response to consecutive optical pulses; b) Evolution of resistance and optical reflectance in response to consecutive electrical pulses applied to a 500nm device.

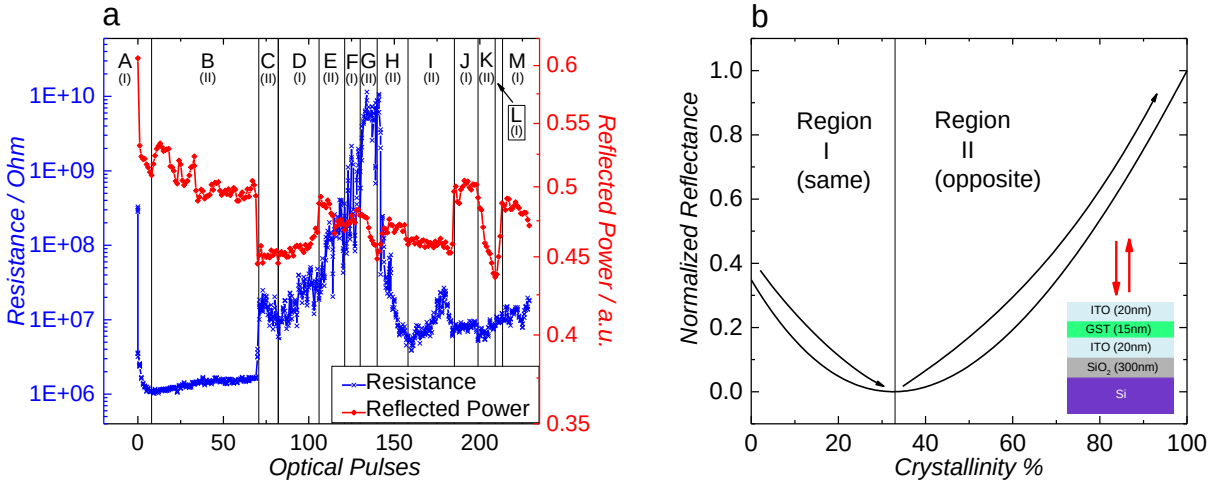

Figure 3. Explanation of the change in reflectance vs resistivity as a consequence of the optical cavity effect (a) Evolution of resistance and reflectance by applying optical pulses, divided into regions where trends either follow or oppose each other; (b) Calculated optical response of the nano-cavity formed by an ITO/GST/ITO crossbar cell as a function of the fraction of crystallized material in the cell. The scale is normalized against the maximum change of reflectance for the specific stack design.

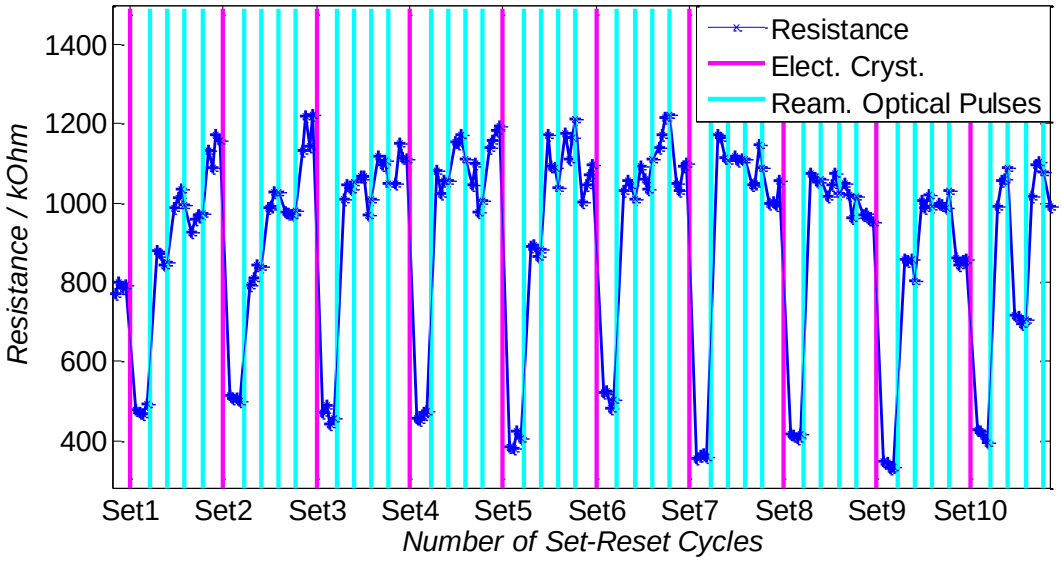

Figure 4. Detail of the change in electrical resistance during 10 iterations of an electrically induced crystallization followed by an optical pulse induced re-morphization.

The table of contents entry

A proof of principle phase-change optoelectronic memory device is demonstrated by encapsulating a thin film of $Ge_2Sb_2Te_5$ between two transparent electrodes. This device allows the study of crystallization of the material when a series of optical and electrical pulses are applied, providing further understanding of phase-change mechanisms for applications in optoelectronic nanodevices.

Keyword: Phase Change Optoelectronics, Mixed-mode operation of phase change devices

G. Rodriguez Hernandez, P. Hosseini, C. Rios, C.D. Wright and H. Bhaskaran*

Title Mixed-Mode electro-optical operation of $Ge_2Sb_2Te_5$ nano-devices

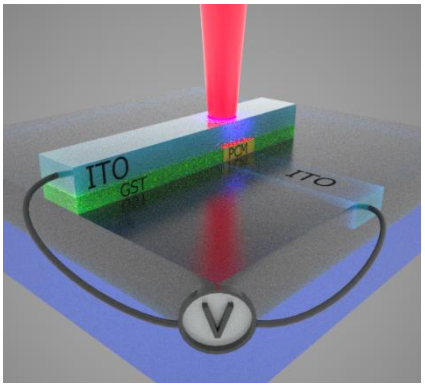

Supporting Information

Mixed-mode electro-optical operation of $Ge_2Sb_2Te_5$ nano-devices

*Gerardo Rodriguez Hernandez, Peiman Hosseini, Carlos Rios, David Wright and Harish Bhaskaran**

1 Procedure to measure the reflectance

The reflectivity of the devices was obtained by capturing a series of images using our home built laser scanning microscope. These images were generated by the Asylum AFM software and contain the intensity of the reflected signal as measured by the photo detector. The value of the reflectance at the device point was extracted by post processing the images. Each data point reported in this paper corresponds to a measurement extracted from an individual image. While extracting the data from the images two factors were required to be corrected to compensate for variations of the system. First of all, the drift of the piezo stage which may be up to 2µm during the duration of the experiment, and second variations in the intensity of the laser caused by temperature fluctuations of the laser diode.

The drift of the images was compensated by an algorithm that extracts four cross sections at different predefined positions of the image to locate the paths of the cross bar device. By identifying the central position of the paths it was possible to accurately determine the center of the crossbar that corresponds to the center of the device. Once the central region was identified, a horizontal cross section over the area of the device was extracted taking the central value of this cross section as the reflectance value of the device at the moment when the image was captured. **Figure S1** shows a characteristic image processed where the center of the device area was identified by the program.

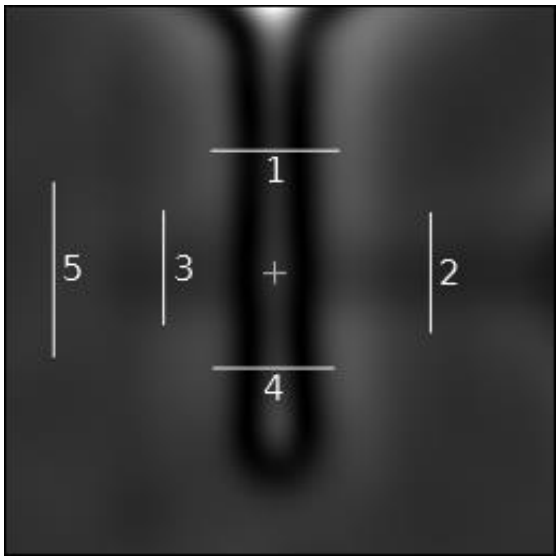

Figure S1. Post processing algorithm for reflectance extraction.

To compensate for the temporal variations of the laser intensity another cross section was extracted, but in this case it corresponds to an area located at a fix distance from the device center where no features exist, only the substrate (Figure S1, line 5). We assume that the reflectance of this reference area does not vary upon phase-change, and therefore any change in the reflectance value of this area accounts for variations of the laser intensity. Further data processing combines the extracted cross sections of the device areas and reference areas, rescaling the intensities of the device areas based on the variations of the average value of reference areas. In order to analyze the variation of the reflectance, each image intensity is rescaled taking as a reference the reflectance of the first image of the series. After rescaling the intensities, the cross sections are re-centered and the central values are extracted, this produces the series that we take as the evolution of the reflectance of the device during the experiment. **Figure S2** shows the before mentioned steps for post processing of the change of reflectance of a typical device.

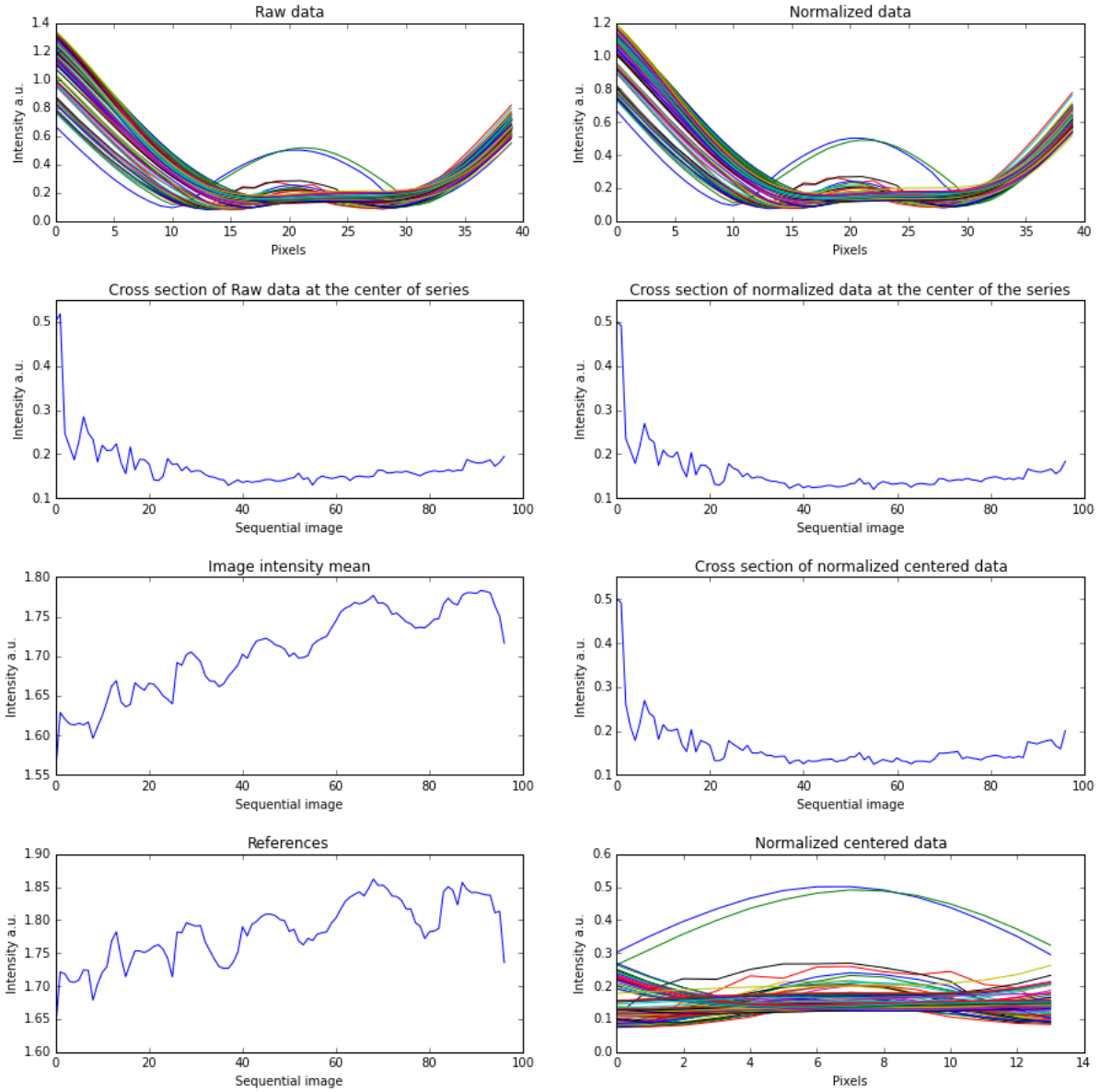

Figure S2. Reflectance extraction post processing steps

2. Optical Stack Model

The optical properties of the devices depend on the thickness of the different layers that form an optical nano-cavity, as was described by Hosseini et al [7]. **Figure S3** shows the designed optical properties at different wavelengths for the optical stack constructed (20nm ITO / 15nmGST / 20nm ITO). It can be seen that at 658nm the fully crystalline state is in fact more reflective than the fully amorphous one. However, **Figure S4** shows the simulated reflectance response of the built optical stack for different possible conditions of *partial crystallization* at 658nm, including the cases when the crystalline and amorphous phase segregate. Figure S4

shows that under any of the possible partial crystallization conditions, a non-monotonic transition occurs. For the discussion, we used the value of bulk crystalline fraction (black line) although experimental data suggest that the crystallization within the device is not homogeneous. However, due to the small differences between responses it was not possible to discriminate which of them better corresponded the experimental data. Nonetheless, this non-linear non-monotonic behavior is responsible for the decrease of reflectance observed upon partial crystallization due to accumulation.

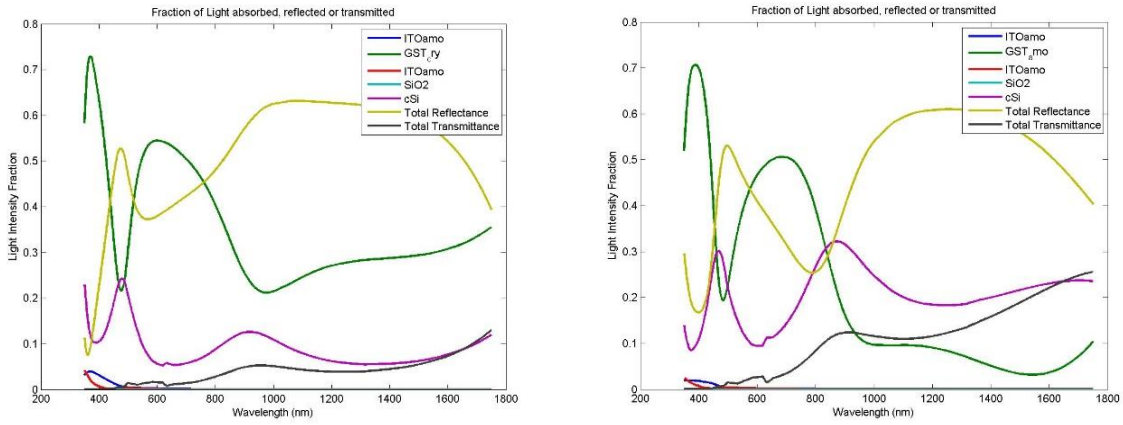

Figure S3. Optical response of the Optical Stack (a) Crystalline (b) Amorphous

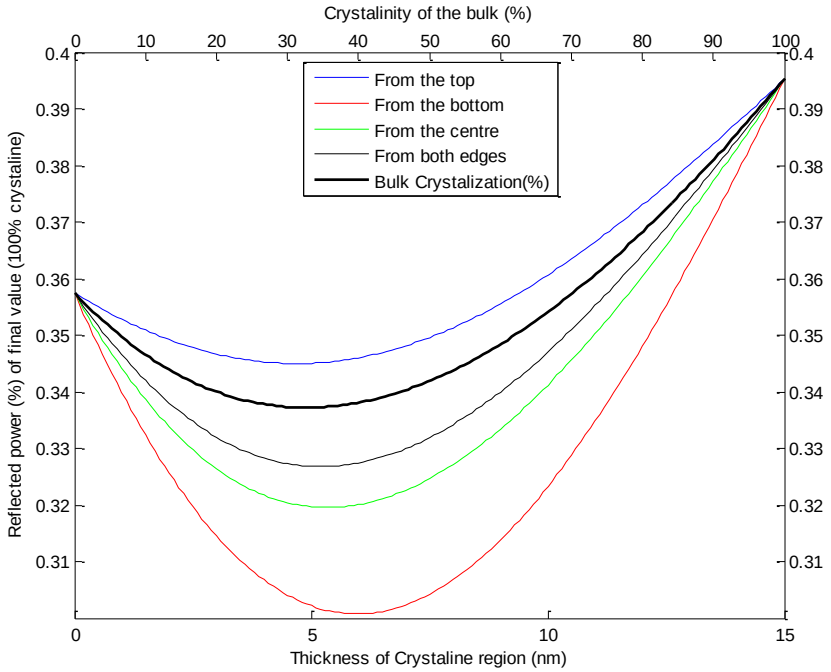

Figure S4. Non-monotonic reflectance response of the optical stack upon different partial crystallization conditions @658nm

3. Mixed-Mode experiment pulse schematics

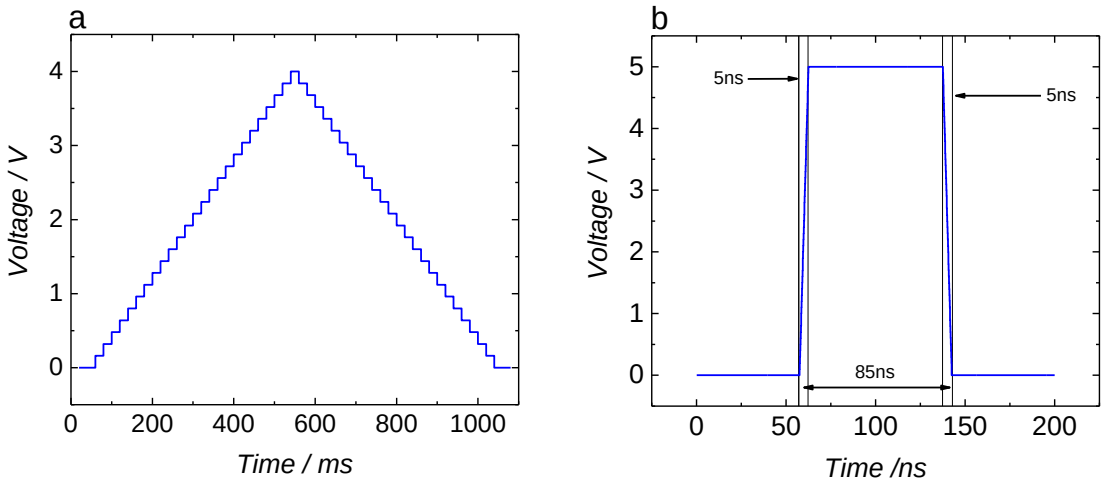

Figure S5. Schematics of pulses used in the opto-electronic memory experiment. (a) Crystallization electrical ramp applied to the device via the electrodes. (b) Individual pulse of the series of 50 pulses, used to drive the laser diode and reamorphize the GST optically.

4. Thermal model of the GST nano-dvices

In order to understand the reduced resistance contrast of the mixed-mode experiment, we performed thermal simulations based on a COMSOL® Multiphysics thermal model. **Figure S6a** shows the 3D geometry of our crossbar devices model. Figure S6b Shows the heat distribution when 65mW of optical laser power are applied to the device. It can be observed that in the top electrode, the heated area exceeds the device region. The reason for this is that the GST is present on the entire top electrode, so the laser light gets absorbed by the GST layer in a circular region of 2.2µm diameter (laser spot size). Figure S6c shows an X,Y plane cross section of Figure S6b with Z at the interface between GST and bottom ITO electrode. It can be seen that a thermal gradient is formed within the device due to heat loss via the ITO bottom electrode (top and bottom square areas of the figure). Such temperature gradient across the device area (black line) is plotted in Figure S6d. It is clear that only the central region of the device reaches the melting temperature of the GST when exposed to 65mW, correspondent to the power limit of our optical system. For this reason, it was not possible to reamorphize the

GST of the entire device, giving as a consequence a low contrast resistance change, operating near the initial crystalline conditions.

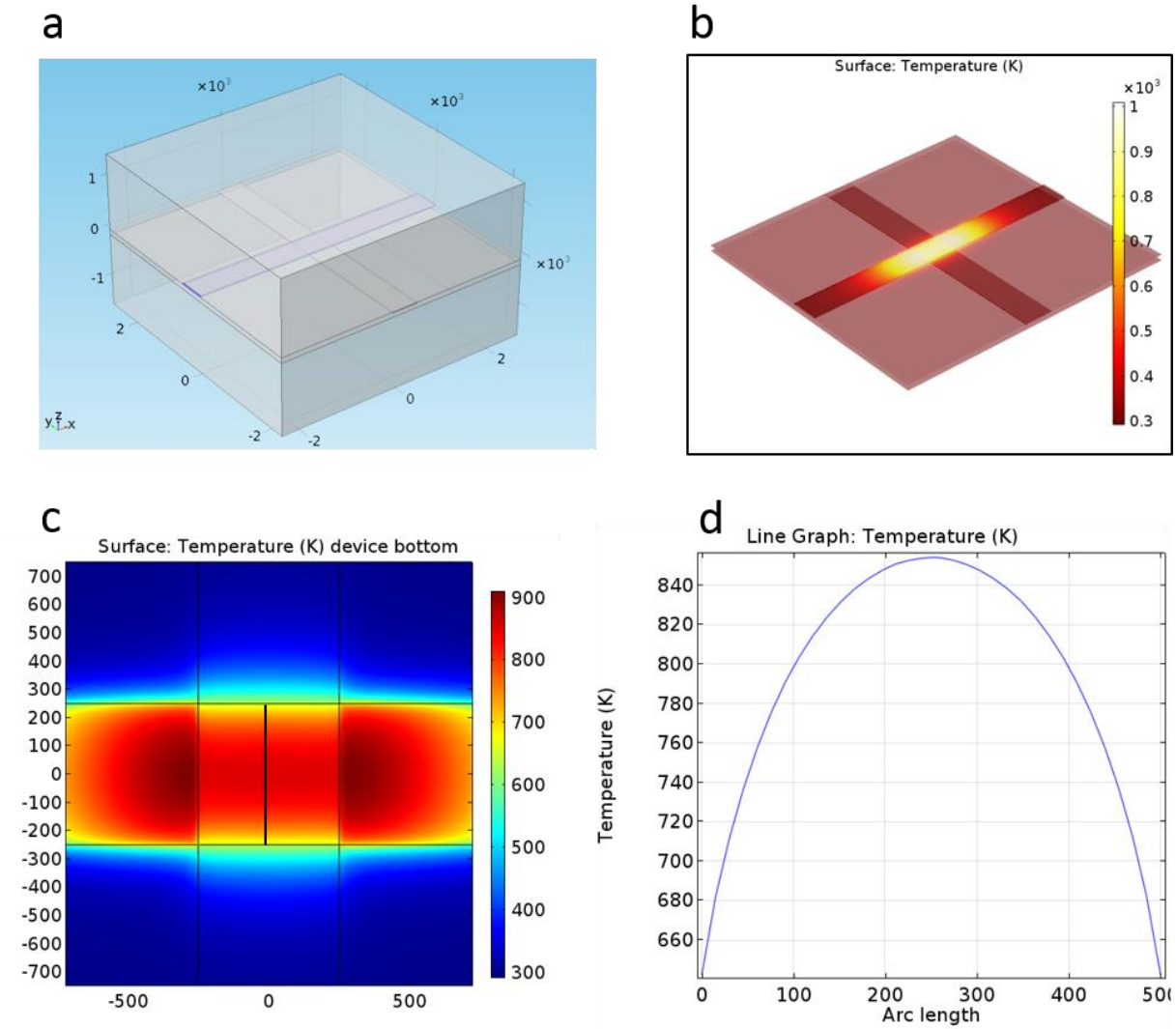

Figure S6. Thermal simulations of a 500 X 500nm device when exposed to 65mW laser power. (a) Schematic of the 3D model. (b)